Carbon Supported Pt+Os Catalysts for Methanol Oxidation

Gülsün Gökağaç[a] and Brendan J. Kennedy[b]

[a] Middle East Technical University, Chemistry Department, 06531, Ankara, Turkey
[b] Department of Inorganic Chemistry, The University of Sydney, Sydney, NSW 2006, Australia

Reprint requests to Assist. Prof. Dr. G. Gökağaç. E-mail: ggulsun@metu.edu.tr

Z. Naturforsch. **57 b,** 193–201 (2002); received July 20, 2001

Methanol Oxidation, Carbon Supported Catalysts, Platinum and Osmium

11% Pt/C, 10% Pt + 1% Os/C, 9% Pt + 2% Os/C, 8% Pt + 3% Os/C, 7% Pt + 4% Os/C, 6% Pt + 5% Os/C and 5% Pt + 6% Os/C catalysts have been prepared for methanol oxidation reaction. Transmission electron microscopy, X-ray photoelectron spectroscopy, X-ray diffraction and cyclic voltammetry have been used to understand the nature of the species present in these catalysts. 7% Pt + 4% Os/C was the most active catalyst, while 8% Pt + 3% Os/C was the least active one. It is found that the metal particle size and distribution on the carbon support, the surface composition and the oxidation states of the metal particles, the metal-metal and metal support interactions are important parameters to define the activity of the catalyst.

1. Introduction

It is apparent that there are a large number of different fuel cells, some of which may be optimised for particular applications [1]. However, the direct methanol fuel cell, DMFC, appears favourable for small scale power generation, such as road transport and portable generators. In spite of the obvious advantages of the DMFC, such as potentially high energy content per unit mass [2], environmental more friendly than any petroleum product, suitable for use in cars and other vehicles [3], methanol's poor electrochemical reactivity in acid solutions except at high potentials limits its use for practical purposes. Therefore, a catalyst is required to activate methanol. At the anode methanol is oxidised to carbon dioxide, and at the cathode oxygen is reduced to water. The overall reaction is:

$$CH_3OH + 3/2\ O_2 \rightarrow CO_2 + 2\ H_2O,\ E^\circ = 1.186\ V\ vs\ SHE.$$

The improvement of effective and low cost catalysts for the electrooxidation of methanol in acid solutions is an essential goal in the development of a practical methanol-air fuel cell. Two complementary approaches are believed to be necessary for the development of practical anodes for metanol electrooxidation: (a) Maximising the effective surface area of the precious metal catalyst, by using a high surface area carbon support, which ensures complete utilisation of all the precious metal [4], (b) the use of a second metal, such as Ru or Sn [5, 6] to promote the formation of active metal oxides at lower potentials and to inhibit the formation of poisons on the surface of the electrode.

Despite the immense amount of work that has been carried out involving unsupported and supported Pt+Ru [4] and Pt+Sn [7] catalysts for methanol electro-oxidation, few studies have been conducted on the carbon supported Pt+Os catalyst system [8]. Therefore, a detailed study of carbon supported Pt+Os catalysts has been undertaken in order to determine the role of osmium on the catalytic activity of methanol electrooxidation.

2. Experimental Section

2.1. Catalyst preparation

1.0 g carbon, Cabot XC-72, was suspended in 400 ml of water and heated to the boiling point. Appropriate amounts of aqueous H_2PtCl_6 and K_2OsCl_6 solutions were added separately followed by sufficient $NaHCO_3$, dissolved in 50 ml of water to neutralise the protons liberated from the acidic metal solutions. The mixture was then boiled for 2 h. Next, a six-fold excess of the reducing agent, formaldehyde, was added and the boiling continued for a further 1 h. The hot catalyst was filtered and washed with a copious amount of boiling distilled water to remove any residual chloride ions, and finally dried at 100 °C in air.

2.2. Electrode preparation

Teflon, Asahi Fluoro Polymer Ltd., 50% by weight teflon, bonded gas diffusion electrodes comprising 27%

teflon and 73% catalysed carbon were prepared by suspending 100 mg of catalysed carbon in 50 ml THF in an ultrasonic bath for 30 min. An appropriate amount of an aqueous suspension of teflon was added dropwise to the rapidly stirred catalysed carbon suspension over 30 min. The water was then removed by repeated washing, 3 - 4 times, and centrifuging the teflon / catalysed carbon slurry with THF. 50 - 70 mg of the teflon / catalysed carbon / THF slurry was deposited onto a 13 mm disc of carbon fibre, Le Carbone-Lorraine TCS 80, and then pressed at 125 kg/cm^2 for 5 min. Finally, the pressed electrodes were dried at 100 °C for 60 min and sintered at 360 °C for 30 min.

2.3. Physical techniques

Transmission electron microscopy studies were performed on a Philips CM 12 fitted with a LaB_6 filament and a lithium drifted silicon detector. The operation voltage was 120 kV. The elemental X-ray microanalysis, energy dispersive X-ray analysis, EDS, was carried out in the CM 12 using the nanoprobe mode. X-ray photoelectron spectra were recorded on a Kratos XSAM 800 spectrometer using K_α lines of Mg, 1253.6 eV, 10 mA as an X-ray source. The main chamber operates in the pressure range of 10^{-9} to 10^{-10} torr. Samples were held in a copper or stainless steel holder with double-sided tape. All lines are referenced to the carbon 1s line at 284.6 eV. An X-ray diffractometer, Siemens D5000 with a Cu anode, was used and NaCl was employed as an internal reference. An Oxsys Micros Potentiostat was used to record cyclic voltammograms and polarisation curves. A mercury / mercury sulfate electrode, MMSE, and high purity platinum gauze were used as a reference and counter electrodes, respectively.

3. Results and Discussion

The polarisation curve results for methanol electrooxidation in 2.5 M H_2SO_4 + 0.5 M CH_3OH at 60 °C are summarised in Fig. 1. The 7%Pt+4%Os/C electrode has the highest short-term activity for methanol oxidation while the 8% Pt + 3% Os/C electrode is the least active. It is immediately apparent from Fig. 1 that the electrocatalytic activities are not a simple function of the Pt:Os ratio but apparently a number of factors such as particle size, crystallite distribution, surface composition, oxidation state of the metals, metal-metal and metal-support interactions are also important.

The particle size and distribution in all samples have been determined before and after electrode

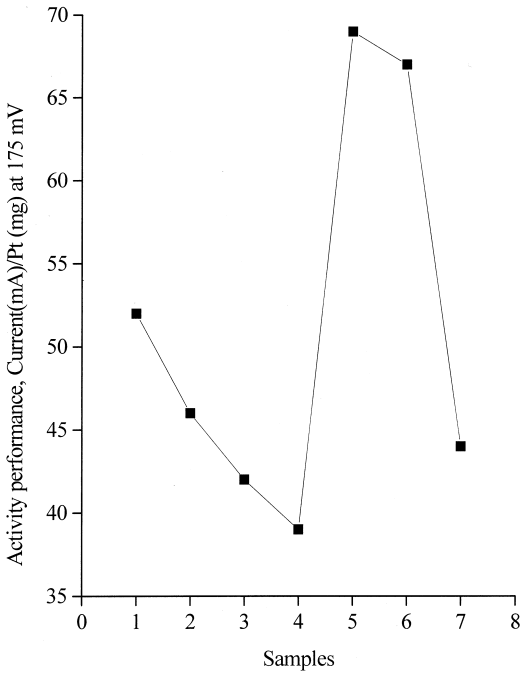

Fig. 1. Short-term polarisation curves of the samples for methanol oxidation at 175 mV in 2.5 M H_2SO_4 + 0.5 M CH_3OH at 60 °C. 1: 11% Pt/C; 2: 10% Pt + 1% Os/C; 3: 9% Pt + 2% Os/C; 4: 8% Pt + 3% Os/C; 5: 7% Pt + 4% Os/C; 6: 6% Pt + 5% Os/C; 7: 5% Pt + 6% Os/C.

fabrication by transmission electron microscopy. Although electrocatalytic measurements were performed using teflon bonded electrodes, it is illustrative to consider the changes resulting from the fabrication process, and accordingly transmission electron micrographs have been recorded for both the as-prepared powder and fabricated teflon bonded electrodes. In part, these measurements were undertaken to confirm that loss of Os as OsO_4 or Os segregation, yielding OsO_2 crystallites, does not occur during electrode fabrication. In a related study, Smith observed that heat treatment of Ru/C electrodes resulted in the formation of RuO_2 crystallites [9, 10]. The major difference between analogous fabricated and unfabricated samples is the increase in the size of the bimetallic crystallites in the actual electrodes presumably as a consequence of sintering of the individual crystallites, since fabrication involves heating the electrodes at 360 °C for 30 min.

The particle sizes of the samples before and after electrode fabrication are summarised in Table 1. Considering firstly as-prepared materials, it is noted that for powder samples of 6% Pt + 5% Os/C and

Table 1. Average particle size of the Pt+Os/C samples.

Samples	As-prepared		Electrode	
	A	B	A	B
11% Pt/C	2.3	8.8	5.0	20.0
10% Pt + 1% Os/C	2.3	–	5.0	20.0
9% Pt + 2% Os/C	2.5	7.5	4.0	14.0
8% Pt + 3% Os/C	2.0	6.0	4.0	20.0
7% Pt + 4% Os/C	1.5	9.0	2.1	10.0
6% Pt + 5% Os/C	2.0	–	2.5	5.0
5% Pt + 6% Os/C	0.9 - 2.5	130	7.0	450

A: Small particles in nm; B: Agglomerated particles in nm.

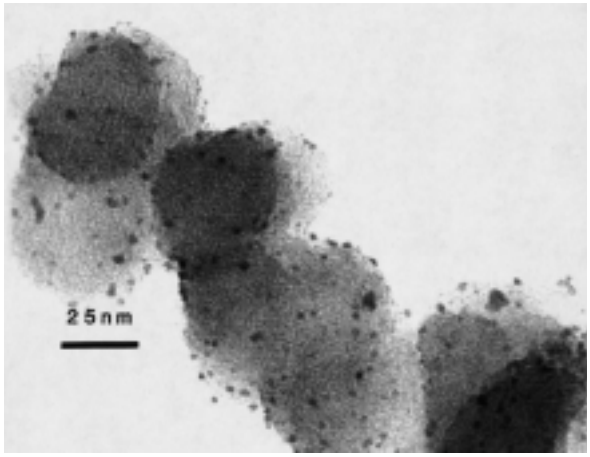

Fig. 2. Transmission electron micrograph of a 10% Pt + 1% Os/C powder sample.

10% Pt + 1% Os/C electrodes, the particles appear to be uniformly distributed on the carbon support, and there is no evidence for agglomeration of the crystallites. For the 10% Pt + 1% Os/C powder sample the majority of the particles are *ca.* 2.3 nm diameter, however there is also evidence for a very small amount of appreciably smaller particles including some down to 1.0 nm, Fig. 2. Electron micrographs of the 6% Pt + 5% Os/C powder sample show a small range of particle sizes between 0.8 and 3 nm diameter without any size dominating. In all other cases, some agglomeration of the crystallites was apparent even before electrode fabrication. For example, as is shown for the 11% Pt/C powder sample in Fig. 3, the majority of the particles are between 1.5 and 3.0 nm in diameter, however, a small number of larger particles *ca.* 7.5 - 10 nm and 25 - 35 nm diameters are also evident. These large crystallites possibly result from the combination of the small individual particles during catalyst deposition. Transmission

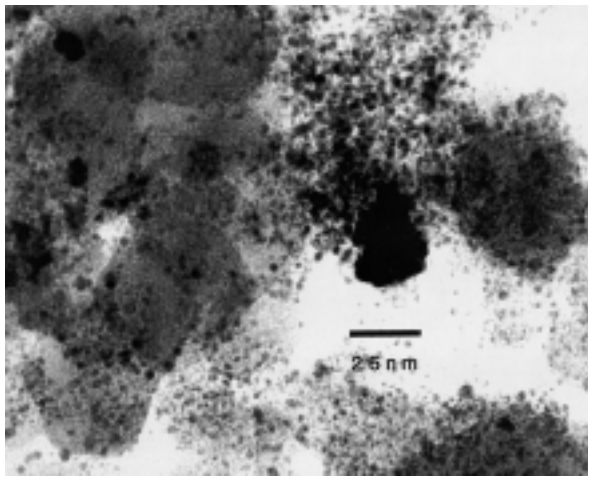

Fig. 3. Transmission electron micrograph of an 11% Pt/C powder sample.

electron micrographs of powder samples of 9% Pt + 2% Os/C, 8% Pt + 3% Os/C and 7% Pt + 4% Os/C, show the particle distribution to be reasonably similar in the three materials. In all three samples, the vast majority of the crystallites are between 1.5 and 2.5 nm diameter and there are also small numbers of somewhat large clusters, 6 - 9 nm, that appear to consist of a number of particles. The 5% Pt + 6% Os/C powder sample shows a different trend to that found in the other powder samples. In this material, almost all the particles are in the range 0.9 - 2.5 nm diameter and there is also a number, albeit small, of extremely large crystallite particles around 125 - 130 nm.

As indicated previously, a major effect of electrode fabrication is the sintering of the metal crystallites. The electron micrographs suggest that the fabricated electrodes can be divided into three groups according to the size of the agglomerated particles. The first group comprises the 11% Pt/C, 10% Pt + 1% Os/C, 9% Pt + 2% Os/C and 8% Pt + 3% Os/C samples. In these samples, the ratio of small to agglomerated particles is seen to differ. For example, the majority of particles present in the 11% Pt/C and 10% Pt + 1% Os/C electrodes are seen to be about 4 - 6 nm in diameter, however there is also a small amount of larger crystallites, *ca.* 15 - 25 nm diameter. Electron micrographs of the 9% Pt + 2% Os/C and 8% Pt + 3% Os/C teflon bonded electrodes show high dispersion of the crystallites even after heat treatment. In general, the majority of the particles in these two samples are between $\sim$2 - 6 nm

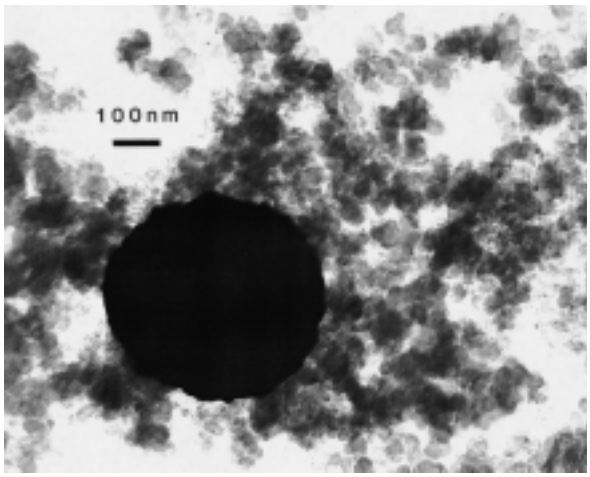

Fig. 4. Transmission electron micrograph of a 5% Pt + 6% Os/C fabricated electrode.

diameter and there are also the large agglomerated particles such as 13 - 15 nm and ∼20 nm diameters for 9% Pt + 2% Os/C and 8% Pt + 3% Os/C, respectively. Micrographs of the 8% Pt + 3% Os/C sample show a very small number of somewhat larger crystallites, *ca.* 40 nm diameter. The second group of electrodes consists of 7% Pt + 4% Os/C and 6% Pt + 5% Os/C. Both electrodes contain agglomerated particles of smaller size with respect to the other samples. Most of the particles are between 1.5 - 3.5 nm and 1.75 - 2.5 nm diameters and there are also large particles, ∼5 nm and 6 - 13 nm diameters 6% Pt + 5% Os/C and 7% Pt + 4% Os/C electrodes, respectively. The final type of distribution is found for the 5% Pt + 6% Os/C electrode. The electron micrographs show that most of the particles are between 6 - 8 nm diameter, and there is a very small number of extremely large particles, up to 450 nm diameter, Fig. 4.

It is now possible to re-examine the catalytic data in terms of variations in the particle sizes observed in the electron microscopy studies. For example, the smallest average particle size is observed for the 7% Pt + 4% Os/C and 6% Pt + 5% Os/C electrodes and these materials have the highest activity for methanol electrooxidation. However, comparing the four samples with particles around 4 - 5 nm diameter, it is apparent that there is a large difference in activity which can not be explained solely in terms of particle size or distribution. Nevertheless, if there is a large difference in crystallite size and / or distribution then the reduced effective crystallite surface area may play a dominant role in determining catalytic activity. This appears to be true for the 6% Pt + 5% Os/C versus 5% Pt + 6% Os/C electrodes where a dramatic difference in reactivity is observed. In 5% Pt + 6% Os/C, not only is the average crystallite size appreciably large, agglomeration has resulted in the formation of a number of extremely large particles further reducing the effective surface area.

X-ray diffraction and EDS analyses were used in an attempt to identify the osmium species present in the Pt+Os samples. With both techniques identification of the osmium species proved difficult. The absence of osmium and / or osmium oxide peaks on the X-ray diffraction pattern could be due to the material having an amorphous structure and/or the small crystallite size in the various samples. Further, if alloying of the Pt+Os occurred a shift in the peak position should be observed in an X-ray diffraction patterns. However, the X-ray diffraction patterns of Pt/C and Pt+Os/C showed only broad peaks typical of platinum presumably as a consequence of the small particle sizes and / or poor crystallinity. The role of the particle size in limiting the ability to find evidence for Os by XRD is supported by the electron microscopy which confirmed the particles to be very small. The absence of strong Os Lα and Kα lines in the EDS is more puzzling. In principle, the small osmium particles should not present any problem in EDS analyses, although obtaining a suitable signal to noise ratio may require analysis over relatively large areas. This constraint appears valid in the present work since for a 10% Os/C sample in which small osmium particles, 0.5 - 2.5 nm diameter are observed the low X-ray count rate precluded obtaining a suitable EDS. For large particles, ∼20 nm diameter, the presence of osmium was rapidly confirmed by EDS. It remains puzzling why mixed Pt/Os particles are difficult to analyse by EDS while X-ray photoelectron spectra, XPS, analysis on identical samples shows appreciable osmium loading.

In order to further characterise the surface composition and hopefully the nature of methanol oxidation on the various samples, cyclic voltammograms in both 2.5 M H_2SO_4 and 2.5 M H_2SO_4 + 0.5 M CH_3OH were recorded. The cyclic voltammograms of all samples in 2.5 M H_2SO_4 are similar, a typical example is shown in Fig. 5, although small shifts in the position of some of the peaks are

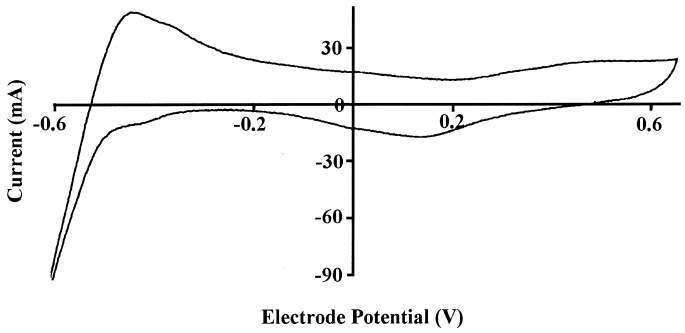

Fig. 5. Cyclic voltammogram of 7% Pt + 4% Os/C in 2.5 M H_2SO_4 at 60 °C. Scan rate 24 mV/sec.

observed. The hydrogen adsorption region of the cyclic voltammograms shows a shoulder due to the formation of an adsorbed hydrogen species, and the rapid increase in cathodic current below this is due to bulk H_2 evolution. There is no evidence indicating that either hydrogen adsorption or evolution are strongly dependent on the Pt:Os ratio. The region above 0 V in the voltammogram is expected to be dominated by metal redox features. For example, the peak observed near 0.1 V in the cathodic scan corresponds to the reduction of Pt-oxides such as:

$$PtO + 2H^+ + 2e^- \rightarrow Pt + H_2O.$$

The potential of this feature, which varies between +0.075 and +0.180 V in the carbon supported Pt+Os electrodes was observed to shift to slightly more positive potential as the Os content was increased with the exception of 9% Pt + 2% Os/C. Another interesting point is the relationship between the Pt-oxide reduction feature near 0 V and the carbon hydroquinone reduction peak. The intensity of the latter feature, relative to that of the Pt-oxide reduction peak, increases with increasing osmium content, possibly indicating decreasing Pt-oxide formation. In the anodic sweep, adsorption of water and oxidation of platinum involves at least three steps:

$$Pt + H_2O \rightarrow Pt\text{-}OH_{ads} + H^+ + e^-,$$
$$Pt\text{-}OH_{ads} \rightarrow Pt\text{-}O_{ads} + H^+ + e^-,$$
$$Pt\text{-}O_{ads} \rightarrow Pt\text{-}O.$$

The adsorption of water on platinum appears as a shoulder in the cyclic voltammograms and it's potential varies between +0.240 and +0.342 V. A feature which can be assigned to the formation of bulk platinum oxide is observed at potentials between +0.420 and +0.560 V. Both features shift to less positive potentials as the osmium content increases but in an irregular order. The largest shift was observed for the 7% Pt + 4% Os/C, 6% Pt + 5% Os/C and 5% Pt + 6% Os/C electrodes indicating that the formation of platinum oxides is easier in these samples.

In all the Pt+Os electrodes no electrochemical response which could be solely ascribed to the presence of osmium was observed. This possibly indicates the absence of any surface Os, which could occur if insertion of the Os into the Pt lattice has occurred. Another explanation for the absence of any osmium redox features is that they are masked by the stronger carbon and/or platinum features. For example, reduction of OsO_2 to Os occurs at ~0 V which falls in the same potential region as the hydroquinone couple [11]:

$$OsO_2(s) + 4\ H^+\ (aq) + 4\ e^- \rightarrow Os(s) + 2\ H_2O.$$

The addition of methanol to the H_2SO_4 electrolyte results in a dramatic change in the appearance of the voltammograms. Examination of the cyclic voltammograms of the samples in 2.5 M H_2SO_4 + 0.5 M CH_3OH indicates that it is possible to separate the materials into two classes. The first class, which comprises 7% Pt + 4 % Os/C, 6% Pt + 5% Os/C and 5% Pt + 6% Os/C, exhibits a classic methanol oxidation response, Fig. 6. Methanol oxidation on platinum electrodes is characterised on the anodic sweep where a weak hydrogen desorption region followed by a reduced double layer region is observed before the onset of methanol oxidation near –0.1 V. Above +0.3 V methanol oxidation is inhibited and the anodic current decreases until the potential is swept into the oxygen evolution region. On the reverse scan, a weak feature corresponding to Pt-oxide reduction is often observed before methanol oxidation recommences around +0.450 V. Around –0.5 V the current again becomes cathodic corresponding to hydrogen adsorption. In these three

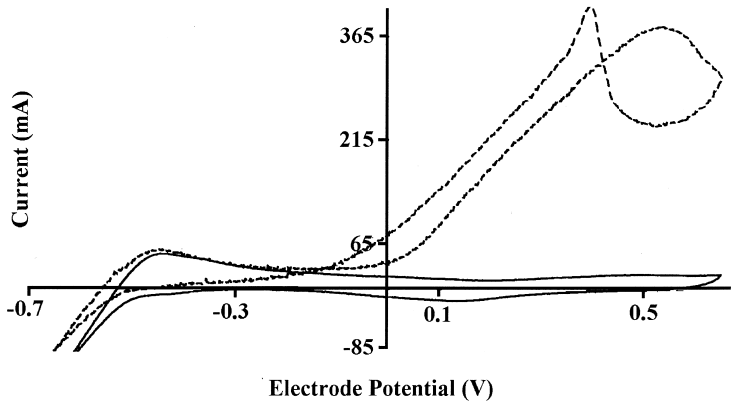

Fig. 6. Cyclic voltammogram of 7% Pt + 4% Os/C in 2.5 MH_2SO_4, (—), and 2.5 M H_2SO_4 + 0.5 M CH_3OH, (- - -), at 60 °C. Scan rate 24 mV/sec.

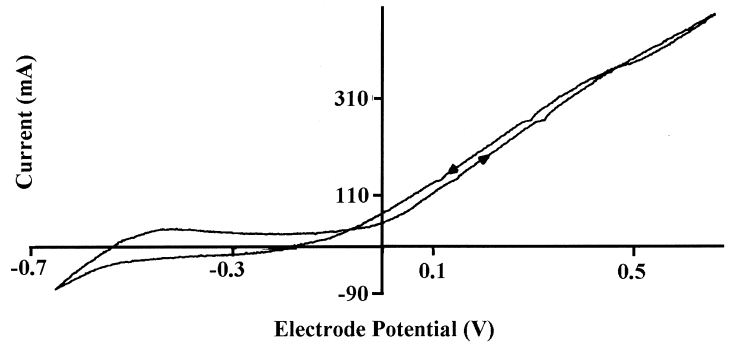

Fig. 7. Cyclic voltammogram of 8% Pt + 3% Os/C in 2.5 M H_2SO_4 + 0.5 M CH_3OH at 60 °C. Scan rate 24 mV/sec.

samples, no structure was observed in the hydrogen region and there was a single desorption feature around –0.45 V. A maximum current density of around 75 mA / Pt (mg) was observed for this class.

The 11% Pt/C, 10% Pt + 1% Os/C, 9% Pt + 2% Os/C and 8% Pt + 3% Os/C electrodes form a second class of materials. For these electrodes the cyclic voltammograms do not show a typical methanol oxidation response. In all these cases, hydrogen desorption is observed between –0.40 and –0.45 V during the anodic sweep. As the potential increases methanol oxidation starts above 0 V, however now there is no limiting current rather, as seen from Fig. 7, the current continues to increase as the potential is swept above +0.60 V, *i. e.*, to the region where O_2 evolution occurs. This possibly shows that methanol oxidation continues to higher potentials at which point oxygen evolution occurs. There is no oxide deactivation. As the scan rate is reversed the anodic current slowly decreases until around –0.5 V where hydrogen adsorption starts. In these materials, a current density of around 150 - 180 mA / Pt (mg), at +0.6 V, is achieved. The difference in behaviour between the two classes appears to be related to the magnitude of the observed current. Simply put, at high current densities a smooth transition to O_2 evolution is observed whereas at lower current densities the rate of Pt-oxide growth is sufficient to inhibit methanol oxidation at intermediate potentials, 0.3 - 0.6 V. It appears that in the second class of materials, any Pt-oxide formed is rapidly consumed by the Pt_3-COH intermediate before it can inhibit methanol adsorption and subsequent oxidation.

X-ray photoelectron spectroscopy has been used in order to obtain information about the composition, environment and relative surface concentrations of all the Pt+Os/C electrodes. In all cases, Pt 4f, Os 4f, O 1s and C 1s spectra were recorded. The C 1s and O 1s lines are, as expected, dominated by the support. In all cases, the Pt 4f lines were poorly resolved $4f_{7/2}$ and $4f_{5/2}$ doublets, Fig. 8. The Pt 4f spectra do not appear as a simple 5/2 - 7/2 doublet, in all cases the apparent $4f_{7/2}$ intensity is much greater than that predicted by either multiplet theory or the relativistic Hatree-Slater atomic model [12]. Deviation from a simple doublet is expected since screening of the core hole by the conduction electron will give rise to asymmetric peak shapes, however, in all the samples the asymmetry is greater than that ob-

Table 2. Pt $4f_{7/2}$ core binding energies, eV, in the Pt+Os samples. The numbers in parentheses are the relative intensities of the species.

Samples	Metal $4f_{7/2}$	Metal-oxide $4f_{7/2}$
10% Pt + 1% Os/C	71.7(67)	73.8(33)
9% Pt + 2% Os/C	71.7(70)	73.7(30)
8% Pt + 3% Os/C	71.9(70)	74.4(30)
7% Pt + 4% Os/C	71.9(50)	74.1(50)
6% Pt + 5% Os/C	71.8(83)	74.0(17)
5% Pt + 6% Os/C	72.0(65)	73.9(35)

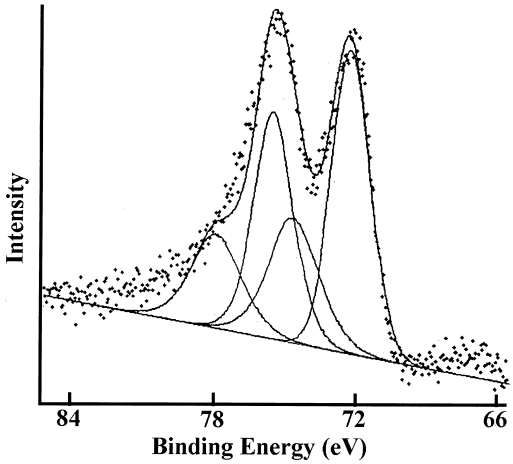

Fig. 8. Pt 4f electron spectra of a 8% Pt + 3% Os/C sample.

served for a clean Pt surface. Considering the Pt+Os sample as an example, spectral fitting, using a pure Gaussian line shape, shows that the bulk of the Pt is present as Pt(0), Pt $4f_{7/2}$ binding energies of 71.7 - 72.0 eV, with a small amount of an oxidised Pt species, Pt $4f_{7/2}$ binding energies of 73.7 - 74.4 eV, Table 2.

It is not possible to determine what oxygen containing groups, O^{2-}, OH^-, or H_2O, are bonded to platinum. In principle, this could be achieved by considering the relative intensity of the platinum 4f and oxygen 1s peaks, however the majority of the oxygen containing groups identified in the XPS are in fact attached to the carbon support. Previously, it has been shown that for $Pt(OH)_4$ the Pt $4f_{7/2}$ E_b is 74.4 eV [13] and for PtO_2 it is 74.6 - 74.9 eV [14]. The binding energy of Pt(II) species is less well established since it is not possible to isolate stable bulk samples of a Pt(II) oxide and hydroxide. Nevertheless, it appears that Pt(II) species have $4f_{7/2}$ E_b of around 72.5 - 73.8 eV [14]. There is also evidence that the platinum binding energy shifts upon

Table 3. Os $4f_{7/2}$ core binding energies, eV, in the Pt+Os samples.

Samples	Os $4f_{7/2}$
10% Pt + 1% Os/C	51.2
9% Pt + 2% Os/C	51.3
8% Pt + 3% Os/C	51.7
7% Pt + 4% Os/C	51.5
6% Pt + 5% Os/C	51.4
5% Pt + 6% Os/C	51.7

formation of species such as a PtO_{ads} to around 72.1 - 72.2 eV [14]. In the current samples the binding energy of oxidised species is indicative of Pt(II), although the exact nature of this species is uncertain. Whilst the main species is undoubtedly Pt(0) the observed binding energy is noticeably higher than that found for either bulk Pt ($4f_{7/2}$ = 71.2 eV) [15] or platinised carbon electrode (Pt $4f_{7/2}$ BE = 71.2 eV) [14, 16, 17]. This shift corresponds to a decrease in the electronic charge density on the Pt atoms present in the Pt+Os/C electrodes. This may indicate that the Os atoms are strongly electron withdrawing in the mixed metal Pt+Os crystallites or it may arise from metal support interactions. Whilst the former explanation is favoured, it is surprising that a stronger dependence of Pt 4f E_b on the Os content is not observed, a point which will be returned to later. The binding energy of the Pt-oxide appears to be independent of the Os content.

The Pt(0):Pt(II) ratio was approximately 7:3 for all samples except 7% Pt + 4% Os/C and 6% Pt + 5% Os/C. In the former case the ratio is around 1:1 demonstrating a higher stability of the oxidised species, whilst for 6% Pt + 5% Os/C the oxide is less stable, the ratio being around 8:2, Table 2. It is unclear what factors determine the relative stability of the surface oxide species except we noted that work of Shukla *et al.* suggests that acidic functional groups on the carbon support promote the formation of surface Pt-oxide species which are believed to be important for methanol oxidation [18]. It should be stressed that XPS is an ex-situ technique, consequently, it is difficult to predict the Pt(0)/Pt(II) ratio on the surface of the electrode during methanol oxidation.

Typically the Os 4f electron spectra appeared as a simple doublet with an Os $4f_{7/2}$ E_b of ~51.3 eV, indicating that Os is present as Os(IV) [8], Table 3. As for the Pt(II) species it is not possible

Table 4. The Pt(0):Pt(II) ratio in bulk and on the surface of the electrode.

Samples	Pt:Os bulk ratio	Pt:Os surface ratio
10% Pt + 1% Os/C	91:9	90:10
9% Pt + 2% Os/C	82:18	90:10
8% Pt + 3% Os/C	73:27	90:10
7% Pt + 4% Os/C	64:36	82:18
6% Pt + 5% Os/C	55:45	82:18
5% Pt + 6% Os/C	45:55	45:55

to distinguish between various Os(IV) formulations including OsO_2, $OsO(OH)_2$, $Os(OH)_4$ and various hydrous salts. Surprisingly, as shown in Table 4 the surface Os:Pt ratio does not smoothly increase as the Os content is increased. For 10% Pt + 1% Os/C, 9% Pt + 2% Os/C and 8% Pt + 3% Os/C the ratio is 90:10. For 7% Pt + 4% Os/C and 6% Pt + 5% Os/C there is a jump in the ratio to 82:18 and for 5% Pt + 6% Os/C the ratio further decreases 45:55. Whilst it is possible that the absolute numbers are in error, since absolute quantification in XPS involves a number of approximations [19], the relative amounts are thought to be well defined. Returning now to the observed Pt(0) 4f 7/2 binding energies a similar jump is observed; that is 10% Pt + 1% Os/C and 9% Pt + 2% Os/C have E_b of 71.7 eV which increases to ∼71.85 eV in 8% Pt + 3% Os/C, 7% Pt + 4% Os/C and 6% Pt + 5% Os/C and again to 72.0 eV in 5% Pt + 6% Os/C. This observation supports the idea that the increase in the binding energy, from that observed in bulk Pt, is as a consequence of electron transfer between the surface Pt and Os atoms either directly or through the carbon support.

Conclusions

Transmission electron microscopy, X-ray photoelectron spectroscopy, X-ray diffraction and cyclic voltammetry results have shown that particle size distribution, surface composition, oxidation state of the metals, metal-metal and metal-support interactions are all important parameters contributing to the activity of the carbon supported Pt+Os catalyst for the electrooxidation of methanol. If only the particle size and distribution are considered, then as observed, it is expected that the 7% Pt + 4% Os/C and 6% Pt + 5% Os/C samples should demonstrate the highest activity for methanol oxidation since these have smaller particle sizes in comparison to the other samples. Similarly, the observed decrease in activity of 5% Pt + 6% Os/C relative to 6% Pt + 5% Os/C may be explained on the basis of the large particles present in the 5% Pt + 6% Os/C electrode.

The Os 4f electron spectra of all the samples show a simple doublet with the Os $4f_{7/2}$ binding energy indicative of Os(IV). The Pt was found in two different oxidation states namely Pt(0) and Pt(II). The Pt(0) binding energy (average ∼71.8 eV) is noticeably higher than that found for other carbon supported Pt (71.2 eV) [16, 17], Pt+Ru (71.2 eV) [8, 17], or Pt+Os (70.9 eV) [8] samples as a consequence of a decrease in charge density on the platinum atoms. Importantly, there is a stepwise increase in the Pt(0) binding energy as the osmium content increases, apparently due to the osmium withdrawing electrons from the platinum.

The platinum-osmium surface composition is different than that of the bulk material. The electrochemical data clearly demonstrate that the surface composition influences the activity of the sample. On the other hand, there appears to be an optimal surface Pt:Os ratio of ∼80:20. At higher Os levels coverage of Pt by an Os-oxide apparently inhibits the adsorption of methanol and consequently decreases the rate of methanol oxidation.

There are two possible pathways for the reaction of a metal oxide with the adsorbed methanol residue during methanol oxidation. The oxide can react either directly with the adsorbed methanol residue or it can promote the formation of an active platinum oxide which subsequently completes the methanol oxidation reaction. In the case of Pt+Ru electrodes, it has been proposed, based on the change in the amount of platinum oxide species on the electrode surface during polarisation, that the second mechanism is valid [8]. For the present Pt+Os/C samples the former pathway appears valid. As shown in Table 2, a substantial Pt(0)/Pt(II) ratio difference between 7% Pt + 4% Os/C and 6% Pt + 5% Os/C samples did not result in any significant difference in activity between these catalysts. Therefore, we suggest that for Pt+Os/C samples the adsorbed methanol fragments react directly with the metal-oxide. It is of course difficult to predict the Pt(0)/Pt(II) ratio on the surface of the electrode during methanol oxidation from ex-situ XPS measurements. All these factors result in a narrow Pt:Os ratio window for enhancement of the methanol oxidation reaction.

[1] K. Kordesch, G Simader, Fuel Cells and Their Applications, VCH Verlagsgesellschaft mbH, Weinheim, Germany (1996).
[2] H. A. Liebhavskky, E. J. Cairns, Fuel Cells and Fuel Batteries, Wiley, New York (1968).
[3] B. D. McNicol, J. Electroanal. Chem. **118**, 71 (1981).
[4] A. S. Arico, A. K. Shukla, K. M. El-Khatib, P. Creti, V. Antonucci, J. Appl. Electrochem. **29**, 671 (1999).
[5] D. Chu, S. Gilman, J. Electrochem. Soc. **143**, 1685 (1996).
[6] C. Lamy, J-M. Léger, S. Srinivasan, in J. O. M. Bockris, B. E. Conway and R. White (eds): Modern Aspects of Electrochemistry, Vol. **34**, pp.53 - 118, Kluwer Academic / Plenum Publishers, New York (2001).
[7] G. Gökağaç, B. J. Kennedy, J. D. Cashion, L. J. Brown, J. Chem. Soc. Faraday Trans. **89 (1)**, 151 (1993).
[8] A. Hamnett, B. J. Kennedy, Electrochim. Acta **33**, 1613 (1988).
[9] B. J. Kennedy, A. W. Smith, J. Electroanal. Chem. **293**, 103 (1990).
[10] B. J. Kennedy, A. W. Smith, F. E. Wagner, Aust. J. Chem. **43**, 913 (1990).
[11] A. J. Bard, R. Parsons, J. Jordan, Standard Potentials in Aqueous Solutions, Marcel Dekker, New York (1985).
[12] J. H. Scofied, Phys. Rev. **179**, 9 (1969).
[13] J. B. Goodenough, A Hamnett, B. J. Kennedy, R. Manoharan, S. A. Weeks, J. Electroanal. Chem. **240**, 133 (1988).
[14] M. Watanabe, M. Uchida, S. Motoo, J. Electroanal. Chem. **229**, 395 (1987).
[15] G. C. Allen, P. M. Tucker, A. Capon, R. Parsons, J. Electroanal. Chem. **50**, 335 (1974).
[16] J. B. Goodenough, A Hamnett, B. J. Kennedy, S. A. Weeks, Electrochimica Acta. **32**, 1233 (1987).
[17] B. J. Kennedy, A. Hamnett, J. Electroanal. Chem. **283**, 271 (1990).
[18] A. K. Shukla, A. Hamnett, A. Roy, S. R. Barman, D. D. Sarma, V. Alderucci, L. Pino, N. Giordano, J. Electroanal. Chem. **352**, 337 (1993).
[19] D. Briggs, M. P. Seah, Practical Surface Analysis, Vol. I, Auger and X-Ray Photoelectron Spectroscopy, John Wiley and Sons Ltd. U. K. (1983).